

## pH dependence of iron photoreduction in a rocky mountain stream affected by acid mine drainage

Diane M. McKnight,<sup>1\*</sup> Briant A. Kimball<sup>2</sup> and Robert L. Runkel<sup>3</sup>

<sup>1</sup> *University of Colorado, Boulder, CO 80303, USA*

<sup>2</sup> *US Geological Survey, Salt Lake City, UT 84104, USA*

<sup>3</sup> *US Geological Survey, Denver, CO 80225, USA*

---

### Abstract:

The redox speciation of dissolved iron and the transport of iron in acidic, metal-enriched streams is controlled by precipitation and dissolution of iron hydroxides, by photoreduction of dissolved ferric iron and hydrous iron oxides, and by oxidation of the resulting dissolved ferrous iron. We examined the pH dependence of these processes in an acidic mine-drainage stream, St Kevin Gulch, Colorado, by experimentally increasing the pH of the stream from about 4.0 to 6.5 and following the downstream changes in iron species. We used a solute transport model with variable flow to evaluate biogeochemical processes controlling downstream transport. We found that at pH 6.4 there was a rapid and large initial loss of ferrous iron concurrent with the precipitation of aluminium hydroxide. Below this reach, ferrous iron was conservative during the morning but there was a net downstream loss of ferrous iron around noon and in the afternoon. Calculation of net oxidation rates shows that the noontime loss rate was generally much faster than rates for the ferrous iron oxidation at pH 6 predicted by Singer and Stumm (1970. *Science* **167**: 1121). The maintenance of ferrous iron concentrations in the morning is explained by the photoreduction of photoreactive ferric species, which are then depleted by noon. Copyright © 2001 John Wiley & Sons, Ltd.

KEY WORDS mountain stream; iron; hydrous metal oxides; photoreduction; reactive transport

### INTRODUCTION

Drainage from abandoned metal mines is a major water quality problem in the Rocky Mountains and Sierra Mountains of the western USA. The weathering of pyrite results in high concentrations of sulfate (SO<sub>4</sub>) and iron (Fe) in mine drainage, whereas high aluminium (Al) concentrations result from acidic weathering of the country rock. Mine drainage may also contribute other metals mobilized by weathering of associated sulfide minerals, including manganese (Mn), zinc (Zn), copper (Cu), cadmium (Cd), and lead (Pb). Streams contaminated by acid mine drainage typically have pH values ranging from 2 to 4 and concentrations of Fe and Al greater than 10<sup>-5</sup> M. The streambeds are covered with abundant deposits of hydrous iron and/or aluminium oxides, which may include poorly crystalline phases containing sulfate (e.g. schwertmanite) as well as some crystalline phases such as goethite and lepidocrocite (Brady *et al.*, 1986; Bigham *et al.*, 1990, 1996). The study of processes controlling metal chemistry in streams receiving acidic mine drainage has been useful in addressing remediation issues, and has provided greater knowledge of Fe biogeochemistry relevant to other aquatic environments.

Photoreduction of dissolved ferric iron (Fe(III)) and hydrous iron oxides is an important process affecting the redox speciation and transport of dissolved Fe in acidic, metal-enriched streams. Low pH enhances the production of dissolved ferrous iron (Fe(II)) by photoreduction because the re-oxidation of Fe(II) by hydroxyl radicals is suppressed and the microbial re-oxidation rate of Fe(II) is also slow. In higher pH environments, where Fe concentrations are typically much lower, photoreduction of dissolved and colloidal hydrous iron

---

\* Correspondence to: D. M. McKnight, University of Colorado, Boulder, CO 80303, USA.

oxides can nonetheless be important in the redox chemistry of other trace species, in altering reactive surfaces of colloidal hydrous iron oxides and in controlling sorption of solutes on oxide surfaces. For example, Kieber and Helz (1992) have shown that in the Chesapeake Estuary, with a pH of 8.4, photoreduction of Fe(III) produces Fe(II), which reacts with chromium(IV) to produce chromium(III), which then precipitates.

Studies of photoreduction to date have focused on iron chemistry in low pH streams (e.g. McKnight and Bencala, 1988; McKnight *et al.*, 1988). Study of photoreduction at neutral pH is motivated by the fact that most remediation plans call for the neutralization of acid mine waters. Further, acidic mine drainage streams that are not subject to remediation often join larger streams with sufficient buffering capacity to neutralize the acid, resulting in circum-neutral pH. In both cases, increases in pH result in the formation of hydrous iron oxides through precipitation reactions. Hydrous iron oxides and dissolved Fe(III) species present in the water column may be exposed to sunlight and subject to photoreduction. Photoreduction may also act on hydrous iron oxides previously deposited on the streambed and stored within the hyporheic zone.

Reactive transport models are important tools for the study of pH-dependent processes that control metal concentrations in acidic mine drainage streams. The ability to simulate pH and trace metal fate and transport provides a framework for the analysis of remediation options. Metal concentrations that result from changes in the quantity and chemistry of mine inflows may be estimated, for example. We have previously developed OTEQ, a reactive transport model that couples physical transport (advection, dispersion, transient storage) with equilibrium chemistry (acid/base reactions, complexation, precipitation/dissolution, and sorption) (Runkel *et al.*, 1996a, 1999). Development of OTEQ was motivated by two stream-scale pH perturbation experiments conducted in acidic mine drainage streams (McKnight and Bencala, 1989; Broshears *et al.*, 1996).

Both pH perturbation experiments included the addition of a conservative tracer (LiCl) that was used to quantify physical transport processes. Addition of an acid or base concurrent with the LiCl addition allowed for the study of pH-dependent reactions in a transport setting. During the first experiment, instream pH was lowered for a 3 h period, resulting in an increase in dissolved iron concentrations (McKnight and Bencala, 1989). Equilibrium-based photochemical dissolution of streambed iron oxides was simulated by considering a trace compartment of recently precipitated oxides and an abundant compartment of aged, less soluble oxides (Runkel *et al.* 1996b). In the second experiment, pH was increased for 5–6 h, resulting in the precipitation of iron and aluminium oxides and the sorption of copper. Reactive transport simulations by Broshears *et al.* (1996) quantified the interactions between pH and hydrous oxide precipitation. Simulation results indicated that the pH increase was buffered by the kinetically controlled desorption of protons from the streambed (Broshears *et al.*, 1996). Sorption of copper was subsequently modeled by Runkel *et al.* (1999) using a surface complexation approach. Analysis of both experiments was limited by a lack of data describing iron redox speciation. As discussed by Broshears *et al.* (1996), further model development is limited by uncertainties in the processes and reaction rates controlling iron redox chemistry as a function of pH.

The objective of the study presented here is to evaluate processes and reaction rates controlling iron redox chemistry in a pH perturbation experiment of longer duration with sufficiently detailed chemical data to provide a direction for future reactive transport model development. Using similar methods as the two previous experiments, we conducted a pH perturbation experiment in which an elevated pH was maintained for 3 days and iron redox speciation was measured. Experimental data were analysed using a conservative solute transport model that considers transient storage and daily flow variation (Runkel, 1998; Runkel *et al.*, 1998). Transport simulations were used to assess whether the oxidation rate of ferrous iron and subsequent precipitation of ferric iron at pH 6.5 was faster or slower than the rate predicted for simple abiotic oxidation of Fe(II) in an oxygenated solution. The net removal rate of Fe was found to be greatly accelerated in the first reach, where hydrous aluminium oxides precipitated, suggesting coupling of removal rates through co-precipitation and/or sorption. In contrast, photoreduction of dissolved Fe(III) or colloidal iron oxides resulted in conservative transport of Fe(II) during the morning in downstream reaches. The analysis of the experimental results suggests further laboratory experiments on coupled Fe and Al precipitation and provides a direction for modelling of Fe redox chemistry in reactive solute transport models.

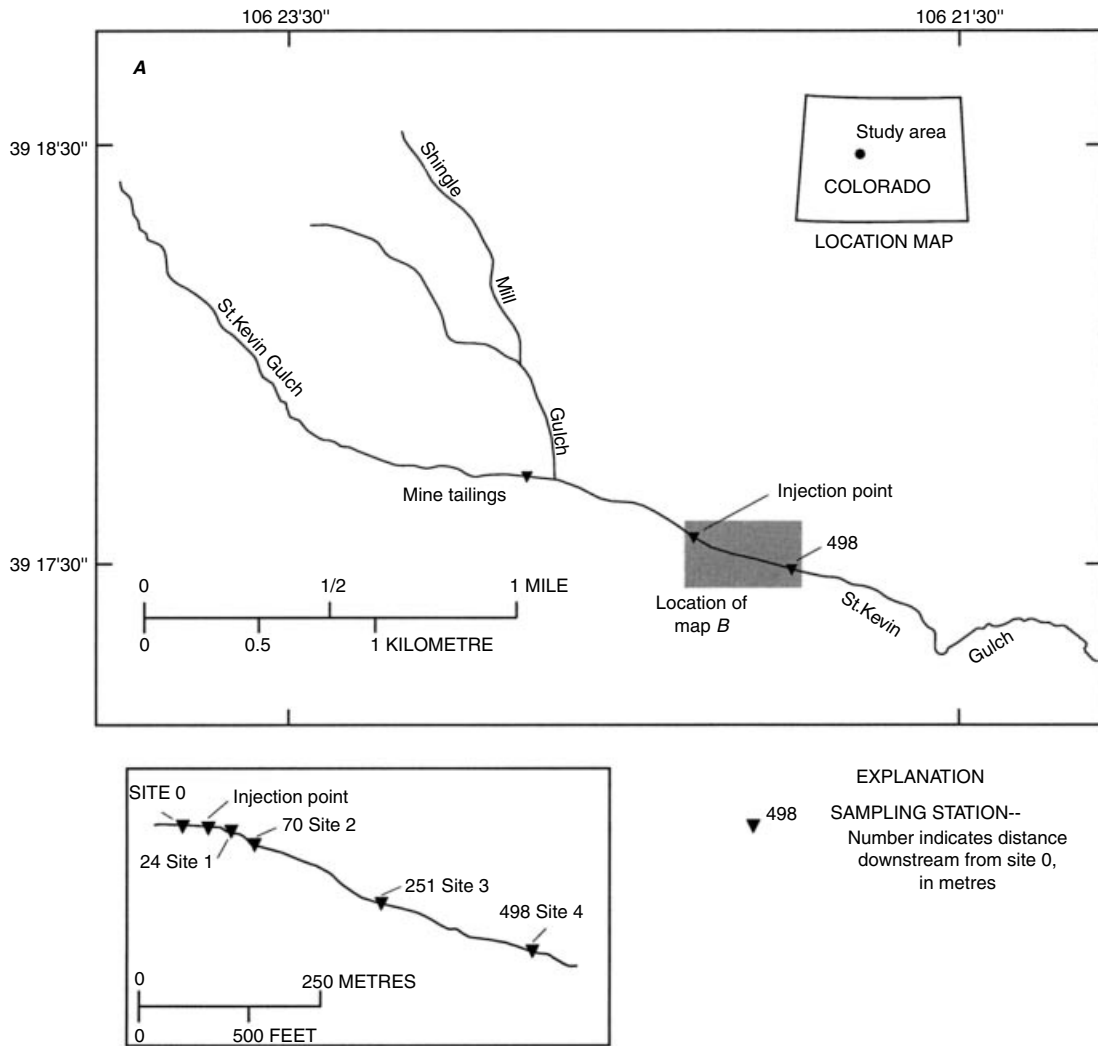


Figure 1. Map of the St Kevin Gulch watershed and the experimental reach where the pH perturbation was conducted

SITE DESCRIPTION AND EXPERIMENTAL METHODS

St Kevin Gulch is a small, mountain stream in Lake County, Colorado, which receives discharge from the Griffin Mine, a lead–zinc mine that ceased operation in the 1920s (Figure 1). Above the mine effluent, stream pH is near 4.6 and Fe and Al concentrations are near 0.5 mg l<sup>-1</sup> and 1.0 mg l<sup>-1</sup> respectively during summer base flow conditions. Below the mine effluent, pH decreases to 3.5 and the concentrations of Fe and Al are about 1.6 and 2.0 mg l<sup>-1</sup> respectively (McKnight *et al.*, 1988; Kimball *et al.*, 1994). Dissolved organic carbon concentrations are approximately 1 mg l<sup>-1</sup> throughout the system (Hrncir and McKnight, 1998). During the summer, abundant populations of a filamentous green alga, *ULOTHRIX* sp., occur in the channel (Tate *et al.*, 1995). Streambed cobble and *ULOTHRIX* filaments are covered by hydrous iron oxides throughout the 2500 m distance from the mine site to where the stream enters a wetland in Tennessee Park. The stream reach immediately downstream from the mine effluent inflow is a zone of active precipitation of hydrous iron oxide and dissolved Fe concentrations decrease exponentially with distance (Kimball *et al.*, 1994). Most of the

stream reaches below the effluent are approximately 2 m wide, and are partially shaded by the forest canopy. In the 250 m reach above the wetland, the stream widens to about 3 m, before splitting to create two channels. The channels in this reach are open and exposed to sunlight. Previous studies have shown that a diel signal of increasing and decreasing Fe(II) can be observed at all sites below the mine effluent (McKnight *et al.*, 1988).

In July 1993, a stream-scale experiment was conducted to quantify Fe reactions at elevated pH (Table I). A continuous injection of a conservative tracer (LiCl) was used to estimate travel time, physical transport parameters, and stream flow (Table II; Bencala *et al.*, 1990). In addition, a base ( $\text{Na}_2\text{CO}_3$ ) was injected to elevate instream pH. Injection rates were monitored throughout the experiment to detect changes in flux rate. The injection site was located approximately 850 m below the mine effluent (Figure 1). Grab samples were collected from the centre of flow immediately above the injection and at four downstream sampling sites (24, 70, 251 and 498 m below the injection site). Samples were composited into 2 l plastic containers that were shielded with aluminium foil to limit exposure to light. Downstream sampling sites were used to define reach endpoints (Table II). Stream flow was measured continuously at a gauging station located at 251 m, and varied with low flows (about  $23 \text{ l s}^{-1}$ ) during the day and higher flows ( $32 \text{ l s}^{-1}$ ) at night (Figure 2a).

Samples for determination of dissolved species were immediately filtered through  $0.1 \mu\text{m}$ , 142 mm diameter, nitrocellulose filters using a peristaltic pump into 125 ml plastic bottles. Samples for cation and metal analysis were acidified with 1 ml Ultrex nitric acid per 125 ml. Shielded tubing and dark plastic bottles were used to minimize the exposure to light. The redox speciation of dissolved Fe (total and ferrous) was assayed immediately after filtration by the 2', 2'-bipyridine method (Brown *et al.*, 1970). The absorbance at 520 nm was determined using a Milton–Roy spectrophotometer within 3 days. The pH was measured immediately upon sample collection using Ross combination pH electrodes and a Beckman pHi 12 pH meter. Anions were

Table I. Sequence of tracer injection activities and sampling in St Kevin Gulch, Colorado

Date	Event
13/7/93	LiCl injection begins (07:52) Diel water quality sampling at background (low) pH
14/7/93	$\text{Na}_2\text{CO}_3$ injection begins (06:51) Diel water quality sampling at experimental (neutral) pH
15/7/93	Diel water quality sampling at experimental (neutral) pH
16/7/93	Injections end (16:27) Diel water quality sampling at background (low) pH
17/7/93	Diel water quality sampling at background (low) pH
18/7/93	Diel water quality sampling at background (low) pH

Table II. Reach definitions, reach travel time, and transient storage parameters

Reach no.	Reach endpoints (m)	Median within reach travel time (min)	Transient storage parameters <sup>a</sup>	
			Storage zone cross-sect. area ( $\text{m}^2$ )	Exchange coefficient ( $\text{s}^{-1}$ )
1	0–24	1.5	0.06	$2.7 \times 10^{-5}$
2	24–70	2.9	0.06	$2.7 \times 10^{-5}$
3	70–251	11.2	0.13	$4.8 \times 10^{-5}$
4	251–498	16.3	0.06	$5.0 \times 10^{-3}$

<sup>a</sup> The dispersion coefficient was set to  $1.0 \text{ m}^2 \text{ s}^{-1}$  for all reaches.

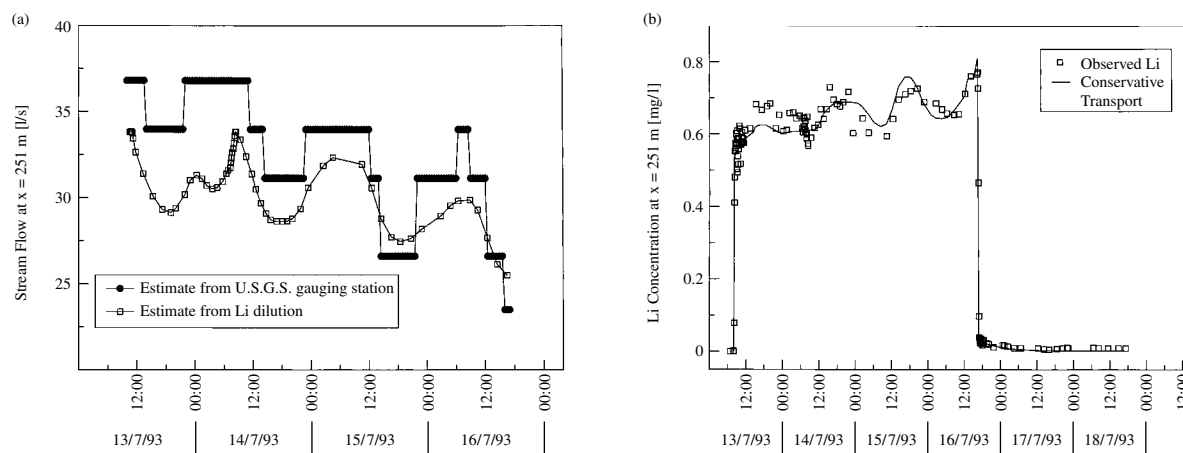


Figure 2. Estimates of stream flow from USGS gauge and tracer dilution (a), observed and simulated Li concentration at 251 m (b)

analysed using a Dionex model 2000 ion chromatograph and cations and metals were analysed using a Jarrel Ash 975 inductively coupled plasma spectrophotometer.

## IRON CHEMISTRY AND SOLUTE TRANSPORT

### *Processes controlling iron chemistry in surface waters with abundant iron oxides*

Chemical and microbial processes that can potentially control Fe concentrations in surface waters with abundant hydrous iron oxides are presented in Table III. For precipitation and dissolution of hydrous iron oxides, the equilibrium concentration of  $\text{Fe}^{3+}$  ion is dependent on  $(\text{OH}^-)$  to the third power for a given value of the solubility product  $K_{s0}$  in reaction (1) (Table III). Thus, small changes in pH can cause large changes in the concentration of  $\text{Fe}^{3+}$  ions. The range in  $K_{s0}$  for amorphous hydrous iron oxides is quite broad and  $K_{s0}$  increases as amorphous iron oxides age.

The exact mechanisms controlling the formation, growth, and deposition of hydrous metal oxides continue to be the subject of active scientific research. At the stream scale, one conceptual model of hydrous iron oxide precipitation involves two steps: (1) formation of polymers, and growth to colloidal particles and (2) aggregation to a particulate size that will settle to the streambed (Grundl and Delwiche, 1993). Grundl and Delwiche (1993) have found that the rates of both processes are first order with respect to the calculated concentration of  $\text{Fe}(\text{OH})_3^0$ . Therefore, for a given concentration of dissolved Fe(III), the rate of precipitation of hydrous iron oxide will be greater at neutral pH than low pH because of the greater importance of  $\text{Fe}(\text{OH})_3^0$  as a dissolved ferric species.

In low pH systems, the oxidation of Fe(II) (reaction (4), Table III) is microbially mediated and can be represented as zero order or first order depending upon assumptions for limitations on microbial growth (Nordstrom, 1985). Because many microbial processes in stream ecosystems are strongly coupled to daily variations in environmental conditions, we have analysed our field experiments in the Snake River, Colorado, by calculating a first-order rate constant ( $k = 0.282 \text{ hr}^{-1}$ ), which is consistent with rates measured in similar environments (McKnight and Bencala, 1988). However, the effective rate constant for microbial oxidation could vary spatially because of patchiness in the distribution of microbial communities in the streambed. In surface waters with pH values above 5.0, abiotic oxidation of Fe(II) is expected to predominate with a rate dependent on pH and Fe(II) concentration, as shown in Equation (4) from Singer and Stumm (1970).

Photoreduction is a chemical process whereby photons in the wavelength range of 360 to 450 nm (ultraviolet radiation) are absorbed by ferric iron species, such as  $\text{FeOH}^{2+}$ , yielding reduced ferrous iron and a radical

Table III. Chemical and microbial processes determining iron chemistry and transport in acidic mountain streams

Process	Reaction	Reaction parameters	Comments
Dissolution and precipitation of hydrous iron oxides	(1) $\text{Fe}(\text{OH})_{3(\text{amorph})} \Leftrightarrow \text{Fe}^{3+} + 3\text{OH}^-$ $\{\text{Fe}^{3+}\}\{\text{OH}^-\}^3 = K_{s0}$	$-\log K_{s0} = 37.3$ to $43.3$ (Stumm and Morgan, 1981)	Heterogeneous reaction for an unstable phase with an apparent solubility product
	(2) $\text{Fe}^{3+} + \text{H}_2\text{O} \Leftrightarrow \text{FeOH}^{2+} + \text{H}^+$ $\frac{\{\text{FeOH}^{2+}\}\{\text{H}^+\}}{\{\text{Fe}^{3+}\}} = \bullet K_1$	$-\log \bullet K_1 = 1.76$	Homogeneous reaction with an equilibrium constant
	(3) $\text{Fe}^{3+} + 2\text{H}_2\text{O} \Leftrightarrow \text{FeOH}_2^+ + 2\text{H}^+$ $\frac{\{\text{FeOH}_2^+\}\{\text{H}^+\}^2}{\{\text{Fe}^{3+}\}} = \bullet K_2$	$-\log \bullet K_2 = -4.79$	Homogeneous reaction with an equilibrium constant
Microbial oxidation of ferrous iron	(4) $\text{Fe}^{2+} \Leftrightarrow \text{Fe}^{3+} + e^-$ $\frac{d\{\text{Fe}^{2+}\}}{dt} = -k\{\text{Fe}^{2+}\}$	$k = 0.282 \text{ h}^{-1}$ , determined in batch experiment (McKnight and Bencala, 1988)	Biologically mediated reaction characterized by an apparent reaction rate
Photoreduction of dissolved ferric iron	(5) $\text{FeOH}^{2+} \xrightarrow{h\nu} \text{Fe}^{2+} + \text{OH}^-$ $\frac{d\{\text{Fe}^{2+}\}}{dt} = R\{\text{FeOH}^{2+}\}$	Solution phase reaction, $R$ is a function of light intensity, light absorption, quantum yield, and reoxidation rate of ferrous iron by hydroxide (David and David, 1976)	Homogeneous reaction characterized by an apparent reaction rate

species, such as  $\text{Fe}^{2+}$  and a hydroxyl radical. The hydroxyl radical can re-oxidize  $\text{Fe}^{2+}$  or can react with other solutes, such as dissolved organic material to produce organic radical species. The ferric species may also be a ferric–organic complex, in which case an organic radical is produced (Voelker *et al.*, 1997). The quantum yield for a photochemical reaction refers to the ratio of the absorbed radiation (moles of photons) to the photoproduct (moles of  $\text{Fe}^{2+}$ ). The solution-phase photoreduction reaction (reaction (5), Table III) is first order with respect to  $\text{FeOH}^{2+}$ . The rate constant  $R$  will depend upon the incident UV-radiation, which can vary temporally and spatially due to shading, and on the quantum yield for the solution-phase reaction. The quantum yield increases at lower pH values because of the slower re-oxidation of  $\text{Fe}(\text{II})$  by hydroxyl radicals. The rate constant for photoreduction of  $\text{Fe}(\text{OH})_2^+$  and  $\text{Fe}(\text{OH})_3^0$ , which are dissolved  $\text{Fe}(\text{III})$  species that become more important at increasing pH, will similarly change with pH. Hydrous iron oxides can be photoreduced as well, with the quantum yield decreasing with increasing crystallinity (Hrncir and McKnight, 1998) and increasing through formation of organic surface complexes on the oxide (Voelker *et al.*, 1997). Hrncir and McKnight (1998) showed that photoreactivity of hydrous iron oxides recently deposited on the streambed of St Kevin Gulch is greater than that of older, more crystalline iron oxides on the streambed, and that a decrease in photoreactivity occurs with 2 to 3 weeks of aging.

#### Quantifying iron transport and transformation

Dissolved iron concentrations observed at each sampling location below the mine inflow result from both physical transport and chemical transformation. Successful interpretation of field data, therefore, requires a thorough understanding of the physical transport processes affecting solute transport in each stream reach. The primary physical processes affecting solute transport in St Kevin Gulch are advection and transient storage. These processes are commonly quantified based on the behaviour of conservative tracers such as chloride and lithium. As described by Broshears *et al.* (1993), lithium concentrations at reach endpoints may be used to determine streamflow by tracer dilution. Under steady flow conditions, estimates of stream cross-sectional area may also be obtained by considering the arrival of the lithium tracer at each reach endpoint. The advective

velocity may then be determined by dividing flow estimates by cross-sectional area. Given the advective velocity, the OTIS solute transport model (Runkel, 1998) may be used to quantify transient storage.

For the 1993 St Kevin Gulch experiment, tracer-dilution estimates and data from the gauging station indicated substantial diel flow variation (Figure 2a). Thus, an unsteady flow routing model was used to determine advective velocity (Runkel *et al.*, 1998). Estimates of the transient storage zone cross-sectional area and exchange coefficient were then determined using OTIS and the observed Li concentration profiles (Table II). Given this description of advection and transient storage, additional OTIS runs were made to simulate the conservative transport of ferrous iron within each reach. Each simulation used the observed ferrous iron concentrations at the end of the preceding reach as the upstream boundary condition. Simulated and observed Fe concentrations at the reach endpoint were then examined to determine whether chemical reactions affected Fe concentrations (i.e. given a reliable description of physical transport, discrepancies between simulated and observed concentrations were attributable to chemical reaction).

A final step in the analysis was to quantify the chemical reactions affecting Fe within the study area. Results from the flow routing analysis were used to identify parcels of water travelling from the injection site to the end of reach 4. Net rates of oxidation were determined for each parcel by integrating Equation (4) (Table III), yielding:

$$C_i = C_0 e^{-kt_i}$$

where  $C_0$  is the ferrous iron concentration at 24 m,  $C_i$  is the ferrous iron concentration at the remaining reach endpoints ( $i = 2, 3, 4$ ),  $t_i$  is the travel time from 24 m to the endpoint of reach  $i$ , and  $k$  is a first-order rate coefficient (McKnight *et al.*, 1988). Estimates of  $k$  for each parcel were determined by regression analysis. Because parcel travel time was not known *a priori*, values of  $C_i$  used within the regression were determined by interpolating between observed data points.

## RESULTS AND DISCUSSION

### *Physical transport*

One of the advantages of employing a solute transport model in conjunction with a conservative tracer is the ability to distinguish between physical and chemical processes. This is especially true for the subject experiment, as the observed changes in stream flow (Figure 2a) can potentially have a large influence on solute concentrations. This hydrologic (physical) influence is exemplified by the variable Li concentrations exhibited at the sampling locations (Figure 2b); due to the effects of dilution Li concentration is inversely related to stream flow. To account for the changes in flow, an unsteady flow routing model was used to simulate the advective velocity used within the OTIS solute transport model. The remaining OTIS parameters describing physical transport were then adjusted such that the observed Li concentrations were reproduced (Figure 2b). Because physical processes affect all solutes equally, the parameters used to quantify Li transport were used to model the conservative transport of Fe(II) as described below. The coupling of the unsteady flow model with OTIS thus provides a framework from which to evaluate the chemical processes affecting iron transport. Additional information on modelling solute transport under unsteady flow is reported by Runkel *et al.* (1998).

### *Downstream changes in pH*

The changes in pH at the downstream sites are shown in Figure 3a. At 24 m, pH rose to 6.0 within 10 min; pH then reached 6.4 after 10 h at 16:48. This slower final rise in pH may be attributed to the desorption of  $H^+$  from the streambed as the pH increased (Broshears *et al.*, 1996). During the remainder of the injection, the pH varied between 6.2 and 6.4; pH dropped rapidly back to 4.2 when the injection was terminated. At the other downstream sites, the initial pH rise occurred in the same time frame as the travel time of the conservative tracer, with the same delay in reaching the maximum pH at about 16:50. The pH increased progressively in the downstream direction, reaching a maximum of 6.6 to 6.8 at 498 m. This increase in pH

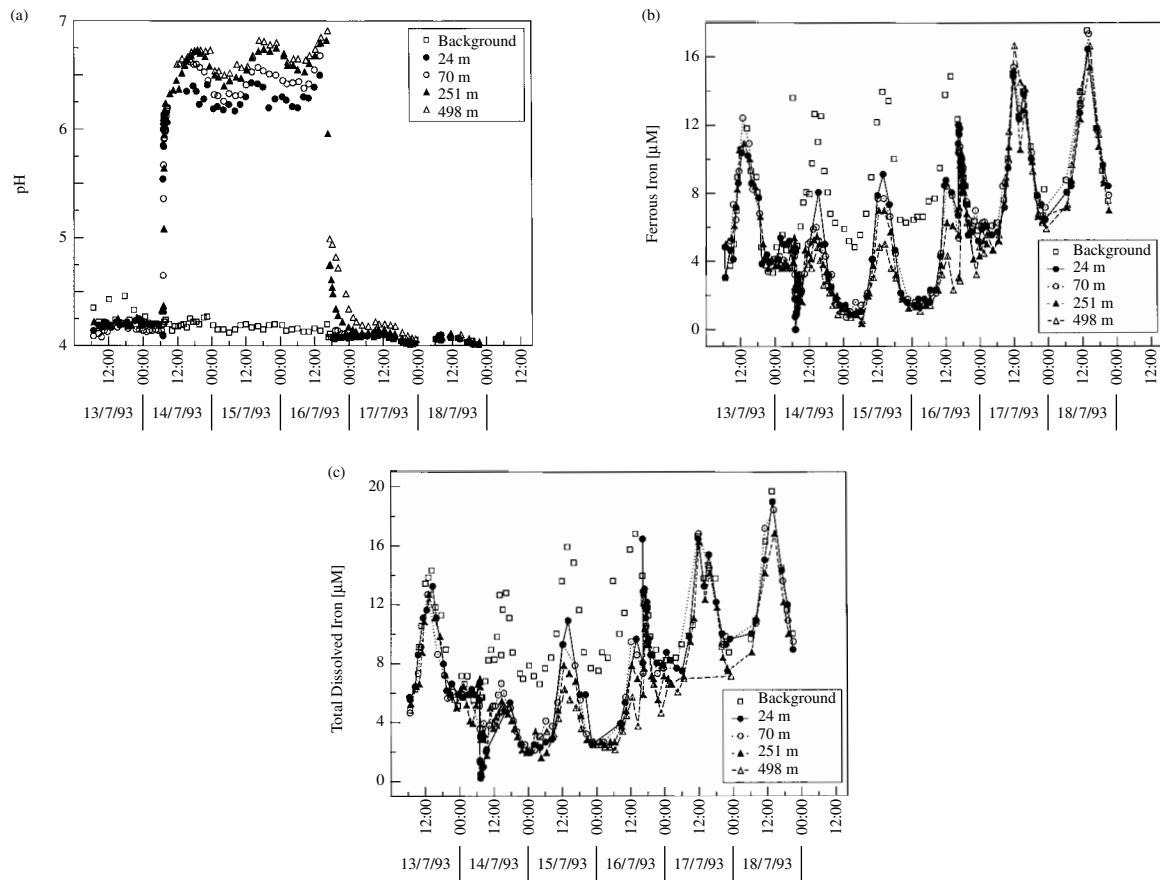


Figure 3. Observed pH (a), ferrous iron (b), and total dissolved iron (c) at downstream sampling sites. The base injection to modify pH began at 06:51 on 14/7/93 and ended at 16:27 on 16/7/93

reflects the degassing of  $\text{CO}_2$  as the stream re-equilibrated with the atmosphere, a process quantified in our analysis of a previous experiment (Broshears *et al.*, 1996).

Superimposed upon the downstream rise in pH is a diel change in pH that is synchronous at the four downstream sites. Between 22:00 and midnight on 14 and 15 July, pH decreased by 0.1–0.2 units at all four sites. This pH decrease corresponds to an increase in flow that diluted the added base. Cool night-time temperatures resulted in decreased evapotranspiration by forest vegetation and an increase in flow.

#### Downstream changes in iron chemistry

Fe(II) and total dissolved iron ( $\text{Fe}_T$ ) concentrations at the downstream sites are shown in Figure 3b and c. Concentration profiles at all sites exhibit a diel pattern in which minimum concentrations are observed just before sunrise and maximum concentrations are observed in the early afternoon. Inspection of background data above the injection site indicates that the diel pattern is independent of changes in pH; pH values at the background site remain relatively constant whereas Fe(II) and  $\text{Fe}_T$  concentrations vary throughout the day (Figure 3a–c). The variations in iron concentration are consistent with a previous study of iron photoreduction in St Kevin Gulch by McKnight *et al.* (1988). Iron concentrations increase throughout the morning hours as hydrous iron oxides on the streambed are photoreduced. Photoreduction decreases in the afternoon hours, as the supply of freshly deposited iron oxides is depleted (Hrncir and McKnight, 1998).

Throughout the experimental increase of pH, Fe(II) accounted for most of the  $Fe_T$ , ranging from 54 to 100%. This result can be explained by two processes. Firstly, most of the dissolved iron entering the upstream reach is ferrous iron because photoreduction maintains high dissolved iron concentrations in the reach below the mine inflows. Secondly, at pH 6.5, Fe(II) is much more soluble than Fe(III), and any Fe(III) produced by Fe(II) oxidation would be expected to precipitate. The fact that dissolved or colloidal Fe(III) species do not become more important species in the downstream direction further indicates that the precipitation and aggregation processes are fast relative to oxidation of Fe(II).

The low concentration of dissolved Fe(III) during the base injection can be understood by considering the speciation of Fe(III) and Al in the stream. Dissolved Fe(III) ( $=Fe_T - Fe(II)$ ) can be present as truly dissolved Fe(III) species ( $Fe^{3+}$ ,  $FeOH^{2+}$ ,  $Fe(OH)_2^+$ ,  $Fe(OH)_3^0$ ) as well as colloidal hydrous iron(III) oxides passing through the 0.1  $\mu m$  filter. At pH 4.2 and Fe(III) concentrations in the range of  $4 \times 10^{-6} M$  (0.2  $mg\ l^{-1}$ ), the two dominant dissolved Fe(III) species are  $FeOH^{2+}$  and  $Fe(OH)_2^+$ . At pH 6.5, the dominant dissolved species is  $Fe(OH)_3^0$ , and iron(III) oxide is predicted to precipitate. From the laboratory results of Grundl and Delwiche (1993), the dominance of the  $Fe(OH)_3^0$  species would be expected to result in optimum conditions for rapid precipitation. In addition to the hydrous iron oxide precipitation, hydrous aluminium oxide is predicted to precipitate at pH 6.5, which is near the pH of minimum Al solubility. Thus, under the conditions of the base addition experiment, hydrous aluminium and iron oxides precipitated rapidly. Further, dissolved Fe(III) essentially became a trace species that was either removed rapidly from the water column by precipitation and aggregation or was photoreduced.

Comparison of  $Fe_T$  and Fe(II) concentrations at the four sites with simulated concentrations based upon conservative transport from the upstream site shows that during the 3 day base injection the first reach was the only reach for which large Fe losses occurred (Figure 4a). In the downstream reaches (reaches 2–4), conservative transport generally accounted for most of the diel variation in Fe(II), especially in the early and mid-morning periods (Figure 4b–d). The conservative simulation results in higher peak Fe(II) concentrations than actually occurred, indicating a continuing downstream loss of Fe(II) at mid-day.

In reach 1, the Fe(II) concentration decreased by 20 to 65% of the value predicted by conservative transport from upstream (Figure 4a). Dissolved Al also decreased dramatically through this reach (Figure 5). The median travel time through this reach was 1.5 min (Table II), indicating that reactions accounting for the removal of Fe(II) were very fast compared with hydrologic transport. Two possible reaction sequences could be invoked to explain the concurrent rapid removal of Fe(II) and Al: (1) Fe(II) could have been rapidly oxidized to Fe(III) and precipitated as hydrous iron oxide or (2) Fe(II) could have been sorbed onto precipitating hydrous aluminium oxide. Removal through oxidation requires three steps: (1) oxidation of Fe(II), (2) formation of colloidal hydrous iron and aluminium oxides, and (3) growth of colloidal oxides to particle sizes greater than 0.1  $\mu m$ . The substantial Al loss indicates that growth was indeed rapid in reach 1. However, unless catalysed in some way, Fe(II) oxidation would be expected to take much longer than 1.5 min. Using an equation that considers the pH dependence of abiotic Fe(II) oxidation (Singer and Stumm, 1970), the calculated rate constant at pH 6.5 is  $0.6\ h^{-1}$  and the observed change in Fe(II) from 14  $\mu M$  to 9  $\mu M$  would be predicted to take 1.1 h. Thus, abiotic oxidation in the absence of a catalyst does not explain the rapid Fe(II) removal in the first reach. The removal is likely due to sorption of Fe(II) by hydrous aluminium oxide or Fe(II) oxidation that was catalysed by the precipitation of oxides providing reactive sites (Scott and Morgan, 1996). However, the first explanation needs to be reconciled with the observation that aluminium oxides found in acidic mine drainage streams are very clean with little iron associated with deposited oxides (Nordstrom, personal communication).

Reach 2 was twice as long as reach 1, with a travel time of 2.9 min. However, the dramatic losses of Fe and Al did not continue in this reach, further indicating the rapidity of the processes in reach 1. In the morning and afternoon of the base injection, Fe(II) transport appeared to be conservative (Figure 4b). For the mid-day period, there was a loss of Fe(II), with Fe(II) concentrations ranging from 70 to 90% of the concentration predicted by conservative transport. The mid-day loss of Fe(II) on the first day of the injection, from 8 to 6.5  $\mu M$ , would be predicted to take 21 min following the Singer and Stumm (1990) equation, much longer

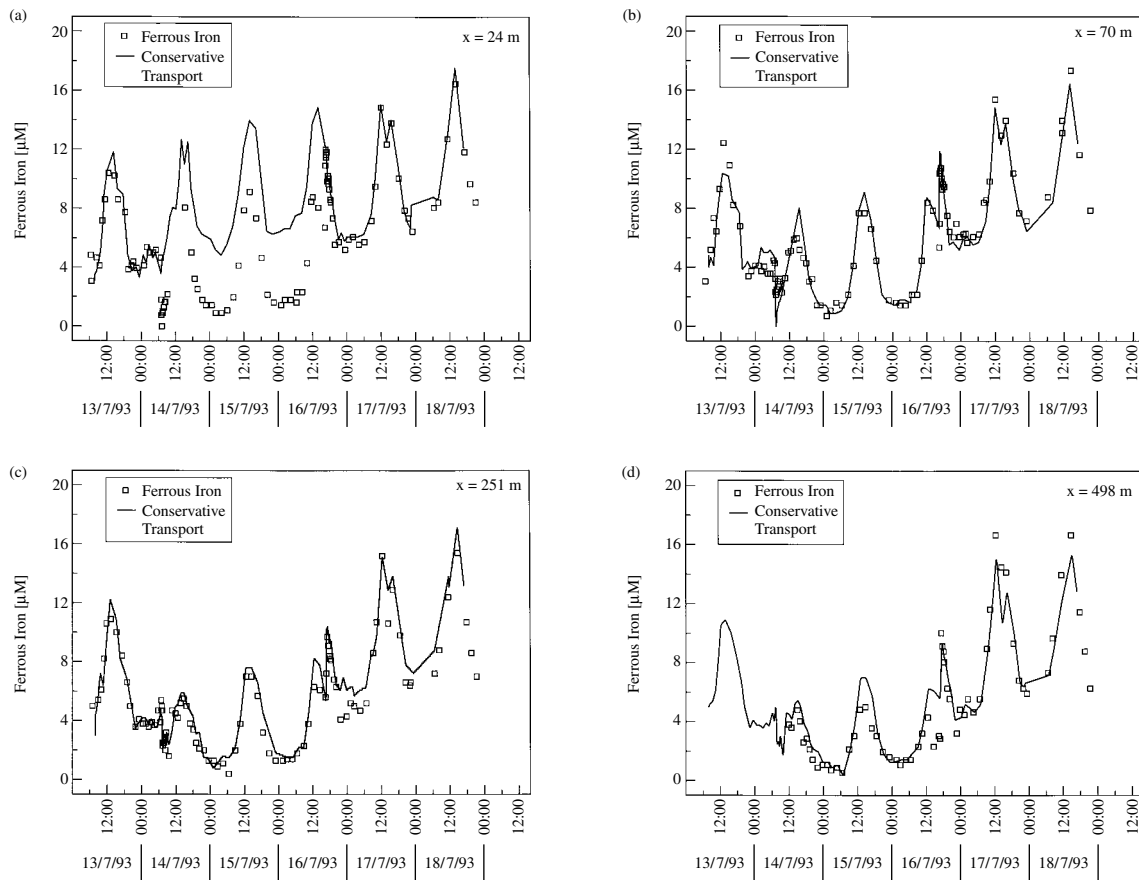


Figure 4. Conservative transport and observed ferrous iron at sites 24 (a), 70 (b), 251 (c) and 498 m below the injection site

than the 2-9 min travel time. This result suggests that at the peak Fe(II) concentrations of mid-day, sorption or co-precipitation reactions continue to enhance removal.

Reach 3 is longer than the previous reaches, with a travel time of 11.2 min. This reach also exhibited conservative transport during mid-morning, and a mid-day loss of Fe(II), occurring between 11:00 and 15:00 (Figure 4c). The longer travel time and the comparable loss suggest that the processes accelerating Fe(II) oxidation and removal as iron(III) hydroxide occur at a slower rate than in the upstream reaches.

Reach 4 has a wide, open channel that is fully exposed to sunlight. With a travel time of 16.3 min, reach 4 is where photoreduction of Fe(III) at neutral pH is most likely to be observed. In mid-morning, Fe(II) did behave conservatively (Figure 4d). However, the Fe(II) concentrations showed a mid-day loss that was greater than the losses occurring in the upstream reaches. The failure of the greater light intensity to cause the rate of photoreduction to match or exceed the rate of oxidation and precipitation suggests photoreduction is limited by the amount of photolabile Fe species in the water column or on the streambed. This interpretation is consistent with the trend of a twofold decrease in photoreactivity of the hydrous iron oxides with distance from the mine effluent that was observed in laboratory experiments (Hrncir and McKnight, 1998).

#### *Photoreduction of dissolved and colloidal iron near neutral pH*

Photoreduction of dissolved Fe(III) and hydrous iron oxides certainly occurred at some rate during the 3 day period of elevated pH. The question of importance for modelling Fe chemistry in surface waters is how

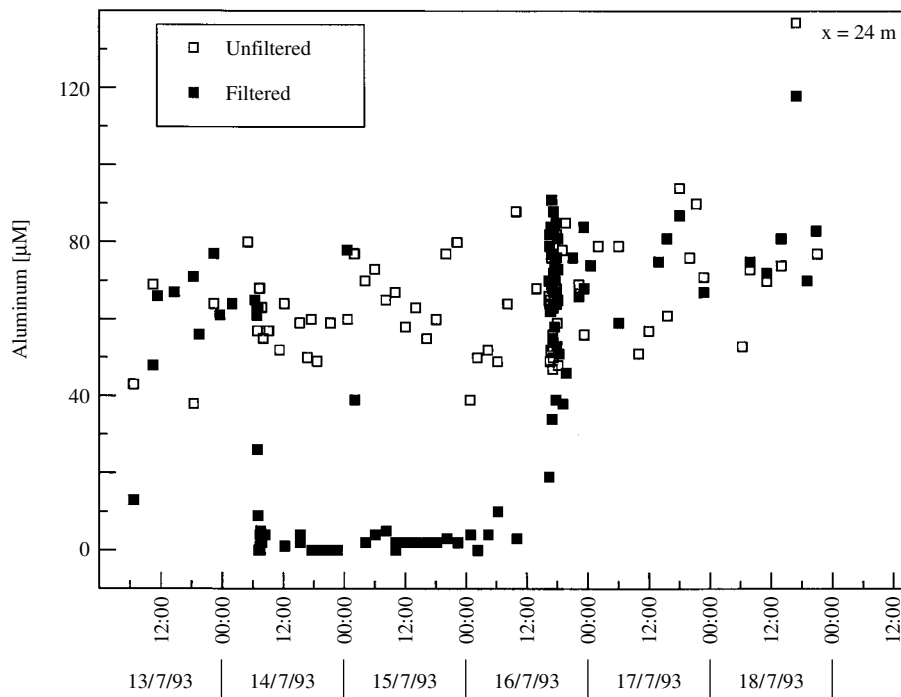


Figure 5. Observed total and dissolved aluminium at 24 m below the injection site

important was photoreduction relative to other processes, specifically Fe(II) oxidation and hydrous iron oxide precipitation or sorption. The analysis of the field experiment shows that during the morning periods the Fe(II) behaved conservatively in reaches 2–4, i.e. Fe(II) loss due to oxidation was balanced by photoreduction of Fe(III). This result suggests that photoreduction is a significant process.

The net oxidation rate constant is plotted *versus* time of day in Figure 6. Positive values of the rate constant correspond to time periods during which oxidation exceeded photoreduction (Fe(II) loss). Conversely, negative values correspond to time periods when photoreduction exceeds oxidation (Fe(II) production). During the base injection, the rate constant increased in the late morning and early afternoon, reflecting an increased loss of Fe(II) (neutral pH, Figure 6). Before and after the base injection, the rate constant remained steady throughout the day, indicating a constant rate of Fe(II) production (low pH, Figure 6). These differences in temporal trends can be explained by differences in the supply of photoreactive Fe(III). Figure 7 shows the net oxidation rate constant as a function of dissolved Fe(III) concentration. At low pH, dissolved Fe(III) concentrations in the water column were high, such that there was an ample supply of photoreducible Fe(III). As a result, the rate constant is negative and photoreduction exceeded oxidation. At neutral pH, Fe(III) concentrations were low and the amount of photoreduction was therefore limited. This is reflected in the positive rate constant, indicating that oxidation exceeded photoreduction. Although dissolved Fe(III) concentrations were low, hydrous iron oxides on the streambed could also be a source of photoreducible Fe(III). The positive rate constants suggest, however, that this alternate source was insignificant. We therefore conclude that dissolved and colloidal ferric iron phases are the primary phases labile to photoreduction at near neutral pH, and that the hydrous iron oxides on the streambed are not photoreactive at near neutral pH to an extent that supplies significant concentrations of Fe(II) to the overlying stream water.

#### *Implications for modelling and remediation of acidic mine drainage*

For the purposes of modeling Fe transport and metals sorbed by hydrous iron oxides, these results indicate that the pH dependence of photoreduction varies among the different solution and solid phases of Fe(III)

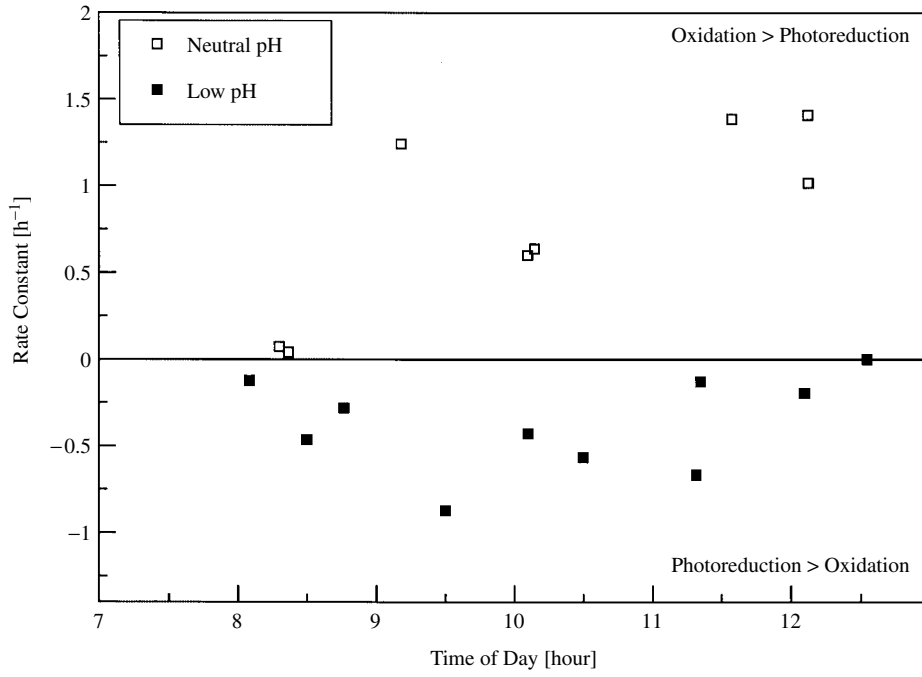


Figure 6. Net oxidation rate constant *versus* time of day for low and neutral pH

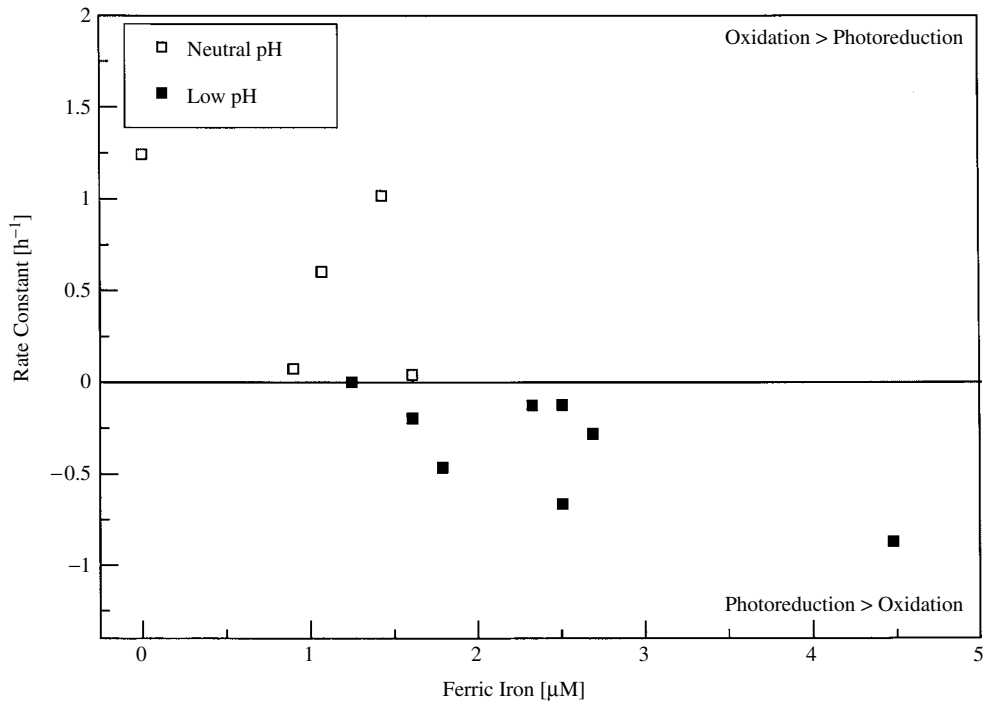


Figure 7. Net oxidation rate constant *versus* dissolved Fe(III) concentration for low and neutral pH

that may be present in surface waters. Dissolved and colloidal Fe(III) species in the water column appear to be photoreactive at near neutral pH; however, the quantum yield is lower than at low pH. On the other hand, photoreduction of recently precipitated hydrous iron oxides present on the streambed does not appear to generate a significant net release of Fe(II) to the water column at near neutral pH. Thus, to model systems of changing pH, it may be simplest to adjust the involvement in photoreductive processes of different phases based upon pH thresholds. These pH thresholds could be determined in laboratory photolysis experiments using well-defined substrates and natural substrates from a stream system under study.

Our results have implications for the outcome of remediation of acidic mine drainage streams. At low pH, photoreduction of streambed oxides not only releases Fe(II) to the stream, but also other species that were sorbed to hydrous iron oxides (Tate *et al.*, 1995). Hydrous iron oxides on the streambed are likely to have sorbed trace contaminants such as Cu and Zn under near-neutral pH conditions. The restriction of significant photoreduction to dissolved and colloidal Fe(III) at near neutral pH suggests that sorbed metals may be effectively sequestered by streambed oxides rather than continually sorbed and released. However, colloidal hydrous iron oxides in the effluent from the acid mine drainage treatment system would be expected to 'turn over' sorbed trace metals.

The experiment in St Kevin Gulch mimicked some aspects of the mixing of acidic mine drainage streams with neutral pH receiving streams. At the base injection site, there was a steady daytime supply of high concentrations of Fe(II) and colloidal iron oxide coming from the upstream reach, which is comparable to a continuous inflow of an acidic mine stream into a larger stream. These results indicate that Fe photoreduction would continue to be a significant process, turning over colloidal oxide surfaces, for example, until a point downstream where all the incoming Fe had been converted to large hydrous iron oxide particles (greater than 0.1  $\mu\text{m}$ ) or actually deposited on the streambed. The downstream concentration and fate of sorbing trace-metal contaminants, such as Cu and Zn, therefore, may be different during the day than at night. These potential differences could be important for designing monitoring programs for acid mine drainage streams and for assessing impacts of metals on the daily cycle of activity of aquatic biota, such as photosynthesis by stream algae and nocturnal drift by benthic invertebrates.

#### ACKNOWLEDGEMENTS

The research described herein was conducted as part of the US Geological Survey's Toxic Substances Hydrology Program. The authors appreciate the helpful review comments of Beth Boyer and Kirk Nordstrom.

#### REFERENCES

- Bencala KE, McKnight DM, Zellweger GW. 1990. Characterization of transport in an acidic and metal-rich mountain stream based on a lithium tracer injection and simulations of transient storage. *Water Resources Research* **26**: 989–1000.
- Bigham JM, Schwertmann U, Carlson L, Murad E. 1990. A poorly crystallized oxyhydroxysulfate of iron formed by bacterial oxidation of Fe(II) in acid mine waters. *Geochimica et Cosmochimica Acta* **54**: 2743–2758.
- Bigham JM, Schwertmann U, Traina SJ, Winland RL, Wolf M. 1996. Schwertmannite and the chemical modeling of iron in acid sulfate waters. *Geochimica et Cosmochimica Acta* **60**: 2111–2121.
- Brady KS, Bigham JM, Jaynes WF, Logan TJ. 1986. Influence of sulfate on Fe-oxide formation: comparisons with a stream receiving acid mine drainage. *Clays and Clay Minerals* **34**: 266–274.
- Broshears RE, Bencala KE, Kimball BA, McKnight DM. 1993. Tracer-dilution experiments and solute-transport simulations for a mountain stream, Saint Kevin Gulch, Colorado. *U.S. Geological Survey Water-Resources Investigations Report 92-4081*. U.S. Geological Survey: Denver, CO; 1–18.
- Broshears RE, Runkel RL, Kimball BA, Bencala KE, McKnight DM. 1996. Reactive solute transport in an acidic stream: experimental pH increase and simulation of controls on pH, aluminium, and iron. *Environmental Science and Technology* **30**: 3016–3024.
- Brown E, Skougstad MW, Fishman MJ. 1970. Methods for collection and analysis of water samples for dissolved minerals and gases. *Techniques for Water Resources Investigations of the United States Geological Survey*, Bk 5; Chapt. A1, 101–105.
- David F, David PG. 1976. Photoredox chemistry of iron (III) chloride and iron (III) perchlorate in aqueous media, a comparative study. *Journal of Physical Chemistry* **80**: 579–583.
- Grundl T, Delwiche J. 1993. Kinetics of ferric oxyhydroxide precipitation. *Journal of Contaminant Hydrology* **14**: 71–97.

- Hrcir DC, McKnight DM. 1998. Variation in photoreactivity of iron hydroxides taken from an acidic mountain stream. *Environmental Science and Technology* **32**: 2137–2141.
- Kieber RJ, Helz GR. 1992. Indirect photoreduction of aqueous chromiim(VI). *Environmental Science and Technology* **26**: 307–319.
- Kimball BA, Broshears RE, Bencala KE, McKnight DM. 1994. Coupling of hydrologic transport and chemical reactions in a stream affected by acid mine drainage. *Environmental Science and Technology* **28**: 2065–2073.
- McKnight DM, Bencala KE. 1988. Diel variations in iron chemistry in an acidic stream in the Colorado Rocky Mountains. *Arctic and Alpine Research* **20**: 492–500.
- McKnight DM, Bencala KE. 1989. Reactive iron transport in an acidic mountain stream in Summit County, Colorado: a hydrologic perspective. *Geochimica et Cosmochimica Acta* **53**: 2225–2234.
- McKnight DM, Kimball BA, Bencala KE. 1988. Iron photoreduction and oxidation in an acidic mountain stream. *Science* **240**: 637–640.
- Nordstrom DK. 1985. The rate of ferrous iron oxidation in a stream receiving acid mine effluent. *U.S. Geological Survey Water-Supply Paper 22780*: 113–119.
- Runkel RL. 1998. One-dimensional transport with inflow and storage (OTIS): a solute transport model for streams and rivers. *U.S. Geological Survey Water-Resources Investigations Report 98-4018*. USGS: Denver, CO; 73.
- Runkel RL, Bencala KE, Broshears RE, Chapra SC. 1996a. Reactive solute transport in streams 1. Development of an equilibrium-based model. *Water Resources Research* **32**: 409–418.
- Runkel RL, McKnight DM, Bencala KE, Chapra SC. 1996b. Reactive solute transport in streams 2. Simulation of a pH modification experiment. *Water Resources Research* **32**: 419–430.
- Runkel RL, McKnight DM, Andrews ED. 1998. Analysis of transient storage subject to unsteady flow: diel flow variation in an Antarctic stream. *Journal of the North American Benthological Society* **17**: 143–154.
- Runkel RL, Kimball BA, McKnight DM, Bencala KE. 1999. Reactive solute transport in streams: a surface complexation approach for trace metal sorption. *Water Resources Research* **35**: 3829–3940.
- Scott MJ, Morgan JJ. 1996. Reactions at oxide surfaces. 2. Oxidation of Se(IV) by synthetic birnessite. *Environmental Science and Technology* **30**: 1990–1996.
- Singer PC, Stumm W. 1970. Acidic mine drainage the rate determining step. *Science* **167**: 1121.
- Stumm W, Morgan JJ. 1981. *Aquatic Chemistry: An Introduction Emphasizing Chemical Equilibria in Natural Waters*. J. Wiley & Sons, Inc.: New York; 780.
- Tate CM, Broshears RE, McKnight DM. 1995. Phosphate dynamics in an acidic mountain stream: interactions involving algal uptake, sorption by iron oxide, and photoreduction. *Limnology Oceanography* **40**: 939–946.
- Voelker BM, Morel FMM, Sulzberger B. 1997. Iron redox cycling in surface waters: effects of humic substances and light. *Environmental Science and Technology* **31**: 1004–1011.